Supplementary information

Gold-based Drug Encapsulation within the Ferritin Nanocage: X-ray Structure and Biological Evaluation as Potential Anticancer Agent of the Auoxo3-loaded protein

Giarita Ferraro,[a] Daria Maria Monti,[a] Angela Amoresano,[a] Nicola Pontillo,[a] Ganna Petruk,[a] Francesca Pane,[a] Maria Agostina Cinellu,[b,c] and Antonello Merlino[a,d*]

[a]*Department of Chemical Sciences, University of Naples Federico II, Complesso Universitario di Monte Sant'Angelo, Via Cintia, I-80126, Napoli, Italy. Fax: +39081674090; Tel: +39081674276; E-mail: antonello.merlino@unina.it*
[b]*Department of Chemistry and Pharmacy, University of Sassari, via Vienna 2, 07100 Sassari, Italy*
[c]*CIRCC, Consorzio Interuniversitario Reattività Chimica e Catalisi, Università di Bari, Via Celso Ulpiani 27, 70126 Bari, Italy*
[d]*CNR Institute of Biostructures and Bioimages, Via Mezzocannone 16, I-80126, Napoli, Italy*

†*Electronic Supplementary Information (ESI) available: See DOI: 10.1039/b000000x†*

Supplementary information

Materials and Methods

Auoxo3 loading into the AFt nanocage

Horse spleen ferritin (Ft) was purchased from Sigma and used without further purification. Auoxo3 was prepared as previously described [1]; it is a *ca.* 1:1 mixture of the *cis* and *trans* isomers. Stock solution of Ft (code F4503) was the same used to prepare the CDDP-encapsulated AFt [2]. The solution was stored at 4 °C in 0.15 mM sodium chloride and contains iron in a protein subunit to metal ratio of 1:26.5, according to inductively coupled plasma mass spectrometry (ICP-MS) measurements.

The Auoxo3-encapsulated AFt was prepared following the procedure previously used to obtain CDDP-encapsulated AFt complex [2]. The loading was achieved by breaking down and then reassembling the Ft nanocage. Briefly, Ft (20 mg x mL^{-1}) was incubated at pH 13 in the presence of Auoxo3 (protein subunit to metal drug molar ratio 1:75); then this mixture was gently slowed down at neutral pH. In particular, the protein sample was slowly raised to pH 13 in the presence of Auoxo3 with 1 M NaOH (final concentration 0.1 M NaOH) and after 30 min, the pH of the resulting solution was adjusted to 7.4 using 1.0 M sodium phosphate buffer. After this process, the sample was extensively centrifuged at 5 000 rpm to remove the abundant precipitates (10 min); then it was recovered and ultra-filtrated (10 kDa cutoff) against 10 mM sodium phosphate buffer, pH 7.4. ICP-MS measurements indicate that Auoxo3-encapsulated Ft contained Au in a 1:8.8 Ft subunit:Auoxo3 ratio, i.e. 1:17.6 Ft subunit to metal ratio, and an undetectable amount of iron, thus the protein is in the Apo form (AFt).

The encapsulation of Auoxo3 in the AFt core was also assessed spectrophotometrically by comparing the UV-Vis spectra of Auoxo3-encapsulated AFt with those of the protein used as control (see below).

Control experiments indicate that Auoxo3 is stable at pH 13. In particular, to control the stability of Auoxo3 at pH 13, 53 mg (0.05 mmol) of the compound were treated with ca. 20 mL of NaOH 0.1 M (pH = 13) and the resulting suspension stirred for 45 min at room temperature, during which the color of the suspension turned from yellow to dark grey. Then the solid product was filtered under vacuum and extracted with MeCN and filtered through Celite to remove some metallic gold. The filtered yellow solution was concentrated to a small volume and diethyl ether added to give 34.6 mg (65 %) of the starting complex, as shown by its 1H NMR spectrum in CD_3CN (Figure S5).

Crystallization and X-ray diffraction data collection

Crystals of Auoxo3-encapsulated AFt with diamond-like morphology, suitable for X-ray diffraction data collection, were grown by hanging-drop vapor diffusion technique at 293 K mixing the protein (5-10 mg x mL^{-1}) with equal volumes of a reservoir solution consisting of 0.6-0.8 M $(NH_4)_2SO_4$, 0.1 M Tris pH 7.4-7.7, 50-60 mM $CdSO_4$.

X-ray diffraction data for Auoxo3-encapsulated AFt were collected from single crystals using a Saturn944 CCD detector equipped with CuKα X-ray radiation from a Rigaku Micromax 007 HF generator at the CNR Institute of Biostructures and Bioimages, Naples, Italy. Crystals were cryoprotected by adding glycerol to the mother liquor (final concentration= 25%) and flash cooled at 100 K. Data sets were indexed, integrated, reduced and scaled using HKL2000 [3] and the indications reported by Karplus and Diederichs [4]. Data collection statistics are reported in Table S2.

Structure resolution and refinement

The structure of Auoxo3-encapsulated AFt was solved by molecular replacement method, using the protein file 5ERK [2], without water molecules and other ligands, as a search probe and the program Phaser [5]. The crystals of this protein were obtained under the same experimental conditions, using a protein sample that was subjected to the same treatment used to encapsulate CDDP [2]. The structure was refined following the protocol used to refine the structure of CDDP-encapsulated AFt with Refmac5.7 [6]. Model building and map inspections were performed using Coot [7]. Gold ions were located if strong signals were observed in the 2Fo-Fc, Fo-Fc and anomalous electron density maps of Auoxo3-encapsulated AFt, but absent in the same positions in the corresponding maps of the starting model, which is a good control [2]. In the assignment of the metal centre, the nature and the arrangement (geometry) of the surrounding atoms were also considered.

To add confidence to out assignments, a detailed comparison of the binding specificity of gold ions versus cadmium ions to amino acids has been performed and the expected metal to ligand atom bond distances have been evaluated considering the standard uncertainties calculated using the 'Calc dpi' webserver [8].

According to statistical analysis carried out using a non-redundant dataset of 195 cadmium-bound proteins, Cd ions have a strong preference for glutamic acid and aspartic acid, although they can also bind the basic amino acid histidine and the polar amino acid cysteine [9]. The distance between Cd ions and atoms belonging to these side chains are on average = 2.3 Å for nitrogen, 2.4 Å for oxygen and 2.5 Å for sulfur [9].

Considering 1) the low affinity for Cd for sulfurs [9], 2) the high affinity of gold for Cys (formation of stable coordinative bonds to soft ligands) [10], 3) the distances between the electron density peaks and sulfur atoms of Cys residues in our structure (1.9 and 2.2 Å), it can be concluded that it is highly probable that Au atoms are bound to Cys48 and Cys126 side chains.

Regarding the binding to ND1 atom of His49 and His132 and NE2 atom His147, the distances between the electron density peaks and N atoms of His side chains are in the range 2.1-2.6 and thus these positions could be in principle occupied by Cd ions.

However, binding of Cd ions to ND1 atom of His49 and His132 and to NE2 atom of His147 is not observed in the crystals of the native protein used as control and in those of the cisplatin-encapsulated adduct grown under the same experimental conditions [2] and even in all the structures of horse spleen ferritin deposited in the protein data bank (see Table S2 in the SI of ref [2]). A comparison of the Cd binding site location in Auoxo3-encapsulated AFt and in previously determined structures of CCDP-encapsulated AFt and of the control, grown under the same experimental conditions used for Auoxo3-encapsulated AFt, are reported in Table S3. As an additional comment, it should be also recalled that gold ions were found close to the side chains of Cys48, His49, His114 and Cys126 also in the X-ray structure of horse liver apo-Ft with $AuCl_4^-$ by other authors (pdb code 3H7G) [11].

A detailed comparison of the native ferritin Cd binding sites and their own anomalous difference map peak heights with the binding sites in the Auoxo3-encapsulated AFt has been also performed. This comparison is reported in Table S4. Considering that gold f " at λ=1.5418 Å is about 1.5 times larger than that of Cd and also considering the analysis performed and discussed in previous paragraphs, we conclude that peaks that we have interpreted as due to Au ions are correctly assigned. We cannot exclude that other peaks, which we have assigned to Cd ions (for example Cd9) could be due to Au. However, since there are known structures of AFt where these positions are occupied by Cd ions (see for example PDB codes 2GYD, 2V2I, 2V2J, 2V2N, 2V2O, 2W0O, 1XZ3) and we cannot confirm Au/Cd replacement, we prefer to put Cd ions in these sites, according to recent guidelines suggested by Helliwell and co-workers: "If you are not sure, do not make an assignment".

The presence of Au ions bound to the protein unambiguously demonstrate that the Auoxo3 compound is broken down. However, to exclude the possibility that the full, starting gold compound could be bound to the protein, the distance between anomalous peaks of our structure was compared to the Au-Au distance observed in the X-ray structure of Auoxo3. Which is close to 3.0 Å [12]. There is only one site where there are two anomalous peaks at a distance comparable with those found in Auoxo3 (3.1 Å, Table S5): This site corresponds to the one where gold atoms are bound to Cys48 side chain. Here, there is not enough space to accommodate the whole Auoxo3 compound. In this respect, it should be also recalled that degradation of Auoxo3 and of other members of Auoxos series upon protein binding has been already observed in previous studies [13-16] and that it is rather well accepted the idea that Auoxos are sensible toward even very mildly reducing conditions, suggesting that they very likely undergo reduction to gold(I) or to colloidal gold upon protein binding.

Refinement statistics are reported in Table S2. Structure validations were carried out using Whatcheck [17]. In the final Fo-Fc difference electron density map, there are 17 peaks whose chemical interpretation is not possible and is commented in Table S6. Coordinates and structure factors of the Auoxo3-encapsulated AFt were deposited in the Protein Data Bank with PDB code 5IX6.

Spectrophotometric measurements

Auoxo3-encapsulated ferritin samples were analyzed by UV-vis absorption spectroscopy with a Cary UV−vis spectrophotometer with temperature controller using a quartz cuvette with 1 cm path length in the range of 240−700 nm. UV-Vis spectra were recorded in 10 mM sodium phosphate pH 7.4 and using the protein at concentration 0.25 mg x mL^{-1}. Data, reported in Figure S3, indicate that gold nanoparticles are probably formed within our sample over time, although in a small amount. Spectra also indicate that Auoxo3-encapsulated ferritin samples are stable for months.

Circular dichroism (CD) spectra were collected on a Jasco spectropolarimeter in the wavelength range 190−250 nm (far-UV) using protein concentration 0.1 mg x mL^{-1} in 10 mM sodium phosphate pH 7.4 (Figure S1).

Hydrodynamic radius (Z-average) of Auoxo3-encapsulated AFt was determined at 25 °C using a Zetasizer Nano ZSP (Malvern Instruments, Malvern, U.K). The average size (Z-average) of fresh solutions of Auoxo3-encapsulated AFt is 13.8 nm, in good agreement with what is found by other authors for cisplatin-encapsulated AFt [18]. Results are the average of three measurements. Aged samples of the Auoxo3-encapsulated AFt are not monodisperse, since they contain the protein and probably variable amounts of gold nanoparticles that can be formed inside the cage (for example a DLS peak centered at 6 nm is sometimes observed).

Inductively coupled plasma mass spectrometry

Protein samples were suspended in 600µl HNO_3 60% and 200µl HCl 37% overnight at 90 °C. Aliquots of acid solution from each sample were directly analyzed by ICP-MS. The solution was then transferred into polystyrene liners, and diluted 1:10 v/v with 5% HNO_3 and finally analyzed with an Agilent 7700 ICP-MS from Agilent Technologies, equipped with a frequency-matching RF generator and 3rd generation Octopole Reaction System (ORS3), operating with helium gas in ORF. The following parameters were used: radiofrequency power 1550 W, plasma gas flow 14 L/min; carrier gas flow 0.99 L/min; He gas flow 4.3 mL/min. 103Rh was used as an internal standard (50 µg x L^{-1} final concentration). Au calibration standards were prepared dissolving Auoxo3 in 5% HNO_3 at 4 different concentrations (1, 10, 50, and 100 µg x L^{-1}). Au concentration was measured. All the analyses were performed as triplicates.

Cytotoxicity, Au uptake and Western blotting analysis

Human breast cancer cells (MCF-7), cervical cancer cells (HeLa), hepatic carcinoma cells (HepG2), human keratinocyte cells (HaCaT), rat cardiomyoblasts cells (H9c2) were from ATCC and were cultured in Dulbecco's modified Eagle's medium (Sigma-Aldrich), supplemented with 10% fetal bovine serum (HyClone,

Logan, UT, USA), 2 mM L-glutamine and antibiotics. The growth medium of H9c2 cells was implemented with 2 mM L-glutamine and 2 mM sodium pyruvate. Human renal cortical epithelial cells HRCE (Innoprot, Biscay, Spain) were cultured in basal medium, supplemented with 2% fetal bovine serum, epithelial cell growth supplement, and antibiotics, all from Innoprot. All cells were grown in a 5% CO_2 humidified atmosphere at 37 °C.

Cells were seeded in 96-well plates at a density of 2.5×10^3/well. 24 h after seeding, cells were incubated with increasing amount of the protein under test (from 12 to 77 μg x mL^{-1}) for 72 h. At the end of incubation, cell viability was assessed by the MTT assay as previously described [19]. Cell survival was expressed as percentage of viable cells in the presence of the analysed protein, with respect to control cells. Control cells are represented by cells grown in the absence of protein and by cells supplemented with identical volumes of protein buffer (10 mM sodium phosphate buffer, pH 7.4).

To investigate Au uptake and to perform western blot analysis, the Auoxo3-encapsulated AFt amount able to induce 50% mortality (IC_{50}) was used. MCF-7 cells were incubated for 24, 48 and 72 h with the Auoxo3-encapsulated AFt and uptake was evaluated as previously reported [20]. Results are reported in Table S7.

To perform western blot analyses, cell lysates were analyzed as previously reported [20]. Results of these analyses are reported in Figure S4. Positive control was obtained by incubating cells in the presence of 50 μg/mL puromycin for 24 h.

References

1. M.A. Cinellu, G. Minghetti, M.V. Pinna, S. Stoccoro, A. Zucca, M. Manassero, M. Sansoni. *J. Chem. Soc., Dalton Trans*. 1998, 1735-1741.
2. N. Pontillo, F. Pane, L. Messori, A. Amoresano, L. Merlino. *Chem. Commun.* 2016, **52**, 4136-4139.
3. Z. Otwinowski, W. Minor, *Methods Enzymol*. 1997, **276**, 307-326.
4. P.A. Karplus, K. Diederichs. *Science* 2012, **336**(6084), 1030-1033; K. Diederichs, P.A. Karplus *Acta Crystallogr D Biol Crystallogr*. 2013, **69** (Pt 7), 1215-1222.
5. A. J. McCoy, R.W.Grosse-Kunstleve, P. D. Adams, M. D. Winn, L.C. Storoni, R.J. Read. *J. Appl. Crystallogr.* 2007, **40**, 658–674.
6. G. N. Murshudov, P. Skubak, A. A. Lebedev, N. S. Pannu, R. A. Steiner, R. A. Nicholls, M. D. Winn, F. Long, A. A. Vagin, *Acta Crystallogr., Sect. D: Biol. Crystallogr*. 2011, **67**, 355-367.
7. P. Emsley, B. Lohkamp, W. G. Scott, K. Cowtan. *Acta Crystallogr D Biol Crystallogr.* 2010, **66**, 486–501.
8. K. S. D. Kumar, M. Gurusaran, S. N. Satheesh, P. Radha, S. Pavithra, K. P. S. T. Tharshan, J. R. Helliwell, K. Sekar. *J. Appl. Cryst*. 2015, **48**, 939–942.
9. R. J. J. Sudan, C. Sudandiradoss. *Acta Crystallogr D Biol Crystallogr.* 2012, 68, 1346–1358.
10. F. Saccoccia, F. Angelucci, G. Boumis, M. Brunori, A. E. Miele, D. L. Williams, A. Bellelli. *J Inorg Biochem*. 2012, 108, 105–111.
11. M. Suzuki, M. Abe, T. Ueno, S. Abe, T. Goto, Y. Toda, T. Akita, Y. Yamada, Y. Watanabe. *Chem Commun*. 2009, 4871-4873.
12. C. Gabbiani A. Guerri, M. A. Cinellu, L. Messori. The Open Crystallography Journal, 2010, 3, 29-40.
13 A. Casini, C. Hartinger, C. Gabbiani. E. Mini, P. J. Dyson, B. K. Keppler, L. Messori. *J Inorg Biochem* 2008, 102, 564-575.
14. I. Russo Krauss, L. Messori, M. A. Cinellu, D. Marasco, R. Sirignano and A. Merlino, *Dalton Trans*., 2014, 43, 17483–17488.
15. L. Messori, F. Scaletti, L. Massai, M.A. Cinellu, C., Gabbiani, A. Vergara, A. Merlino. Chem Commun (Camb). 2013, 49, 86, 10100-10102.
16. L. Messori, M. A. Cinellu, A. Merlino. *ACS Med Chem Lett*. 2014, 5, 10, 1110-1113.
17. R.W.W. Hooft, G. Vriend, C. Sander, E. E. Abola, *Nature* 1996, **381**, 272.
18. (a) M. Uchida, M. L. Flenniken, M. Allen, D. A. Willits, B.E. Crowley,S. Brumfield, A. F. Willis, L. Jackiw, M. Jutila, M. J. Young, T. Douglas. J. Am. Chem Soc. 2006, 128, 16626-33; (b) E. Falvo, E. Tremante, R. Fraioli, C. Leonetti, C. Zamparelli, A. Boffi, V. Morea, P. Ceci, P. Giacomini. Nanoscale, 2013,5, 12278
19. R. Del Giudice, A. Raiola, G. C. Tenore, L. Frusciante, A. Barone, D.M. Monti, M.M. Rigano. *J. Funct. Foods*. 2015, **18**, 83-94.
20. E. Galano, A. Arciello, R. Piccoli, D. M. Monti, A. Amoresano. *Metallomics*, 2014, 6, 587--597

Table S1. Interactions between Au atoms and protein residues or solvent atoms in the structurte of Auoxo3-erncapsulated AFt.

Binding site	Distance (Å)	Angle (°)
Cys48 and His49		
Au2-SG Cys48	1.9	
Au6- centroid His49	3.2	
SG Cys48-Au6-centroid His49		152.5
Au6-SG Cys48	2.3	
Au2-Au6	3.1	
His49		
Au3-ND1 His49	2.1	
Cys126 and His114		
Au1-SG Cys126	2.2	
Au1-ND1 His114	2.2	
SG Cys126-Au1-ND1 His114		178.6
Au4-SG Cys126	2.2	
Au4-O Wat	2.5	
SG Cys126-Au4-O Wat		173.1
Au1-Au4	3.7	
His132		
Au7-ND1 His132	2.5	
His147		
Au5-NE2 His147	2.6	

Unrestrained selected bond distances and angles are in Å and °, respectively. Standard uncertainties on the coordinates 0.1 Å. Errors on distances<0.2 Å

Table S2. Data Collection and refinement statistics

Data reduction	
PDB code	5IX6
Space group	F432
Unit cell parameters	
a=b=c (Å)	180.645
Molecules per asymmetric unit	1
Observed reflections	151428
Unique reflections	22027
Resolution (Å)	104.30-1.85 (1.88-1.85)
Completeness (%)	99.5 (95.0)
Anomalous completeness (%)	99.2 (88.1)
Rpim in top intensity bin	0.032
Rpim	0.102 (0.659)
I/σ(I)	9.2 (0.8)
Multiplicity	6.9 (3.4)
$C_{1/2}$ last shell	0.284
CC*	0.666
Refinement	
Resolution (Å)	104.30-1.85
number of reflections in working set	20893
number of reflections in test set	1128
R-factor/Rfree/Rall (%)	18.0/18.2/22.6
Non-H atoms used in the refinement	1785
Mean B-value (Å^2)	19.7
Au atom occupancy	0.40, 0.30, 0.35, 0.45, 0.25, 0.45 and 0.20
Au atom B-factor (Å^2)	20.0, 34.8, 29.5, 20.6, 38.9, 38.7 and 50.5
Estimated overall coordinate errors	
Rmsd bonds (Å)	0.019
Rmsd angles (°)	1.77
Ramachandran values (%) from Coot	
Preferred region	96.32
Allowed	2.94
Disallowed	0.74 (1 residue:Ser157)

Parentheses indicate information for highest resolution shell.

Table S3. Interactions of Cd^{2+} ions in Auoxo3-encapsulated AFt, CCDP-encapsulated AFt and in the control

Auoxo3-encapsulated AFt	Auoxo3-encapsulated AFt	CDDP-encapsulated Aft and Control	CDDP-encapsulated AFt	Control	CDDP-encapsulated AFt (crystal 2)
Atom	Interactions at distance < 3.00 Å	Atom	Interactions at distance < 3.00 Å	Interactions at distance < 3.00 Å	Interactions at distance < 3.00 Å
CD1	Occupancy 0.40 B-factor 40.5 Å^2 OE1 Glu11 (2.6 Å) OE2 Glu11 (2.8 Å) WAT 129 (2.2 Å) WAT 384 (2.7 Å) WAT 399 (2.8 Å) WAT 447 (2.2 Å)	CD1	Occupancy 0.40 B-factor 22.9 Å^2 OE1 Glu11 (2.3 Å) OE2 Glu11 (2.6 Å) WAT 129 (2.2 Å) WAT 183 (2.3 Å) Cl 3 (2.60 Å)	Occupancy 0.40 B-factor 42.4 Å^2 OE1 Glu11 (2.7 Å) OE2 Glu11 (2.3 Å) WAT 129 (2.8 Å) WAT 319 (2.6 Å) Cl 3 (2.5 Å)	Occupancy 0.40 B-factor 41.4 Å^2 OE1 Glu11 (2.7 Å) OE2 Glu11 (2.5 Å) WAT 129 (2.0 Å) WAT 183 (2.6 Å) Cl 4 (2.6 Å)
CD2	Occupancy 0.45 B-factor 58.66 Å^2 OE1 Glu56 (2.5 Å)	CD2	Occupancy 0.40 B-factor 43.7 Å^2 OE1 Glu53 (2.9 Å) OE2 Glu53 (2.4 Å) OE1 Glu56 (2.5 Å) WAT 237 (2.5 Å)	Occupancy 0.30 B-factor 51.9 Å^2 OE1 Glu53 (2.5 Å) OE2 Glu53 (2.6 Å) OE1 Glu56 (2.5 Å) WAT 315 (2.3 Å)	Occupancy 0.40 B-factor 51.8 Å^2 OE1 Glu53 (2.9 Å) OE2 Glu53 (2.9 Å) OE1 Glu56 (2.4 Å) WAT 302 (2.9 Å)
CD8	Occupancy 0.40 B-factor 41.9 Å^2 OE1 Glu60 (2.8 Å) OE2 Glu60 (2.4 Å) OE1 Glu56 (2.7 Å) OE2 Glu57 (2.7 Å) WAT 471 (2.5 Å)	CD3	Occupancy 0.30 B-factor 44.0 Å^2 OE2 Glu56 (2.4 Å) OE1 Glu60 (2.8 Å) OE2 Glu60 (2.2 Å) Occupancy 0.20 B-factor 35.80 Å^2 OE1 Glu60 (2.4 Å) WAT 191 (2.2 Å)	Occupancy 0.30 B-factor 69.1 Å^2 OE1 Glu60 (2.5 Å) WAT 292 (2.8 Å)	Occupancy 0.30 B-factor 56.4 Å^2 OE2 Glu56 (2.9 Å) OE1 Glu60 (2.8 Å) OE2 Glu60 (2.7 Å) Occupancy 0.20 B-factor 60.5 Å^2 OE1 Glu60 (2.4 Å) WAT 191 (2.4 Å) Cl 6 (2.7 Å)
CD3	Occupancy 0.50 B-factor Å^2 OD1 Asp80 (2.4 Å) OD2 Asp80 (2.2 Å) OD1 Asp80* (2.4 Å) OD2 Asp80* (2.2 Å) WAT 386 (2.4 Å) WAT 386* (2.4 Å)	CD4 at the binary axis	Occupancy 0.40 B-factor 10.5 Å^2 OD1 Asp80 (2.3 Å) OD2 Asp80 (2.5 Å) OD1 Asp80* (2.3 Å) OD2 Asp80* (2.5 Å) Cl 1 (2.4Å) Cl 1* (2.5 Å) Occupancy 0.10 B-factor 19.5 Å^2 OD1 Asp80 (2.1 Å) OD2 Asp80 (1.9 Å) OD1 Asp80* (2.2 Å) OD2 Asp80* (2.1 Å) Cl 1 (2.9 Å)	Occupancy 0.50 B-factor 15.7 Å^2 OD1 Asp80 (2.4 Å) OD2 Asp80 (2.1 Å) OD1 Asp80* (2.5 Å) OD2 Asp80* (2.3 Å) Cl 2 (2.6 Å) Cl 2* (2.3 Å)	Occupancy 0.50 B-factor 16.4 Å^2 OD1 Asp80 (2.5 Å) OD2 Asp80 (2.2 Å) OD1 Asp80* (2.5 Å) OD2 Asp80* (2.4 Å) Cl 1 (2.5 Å) Cl 1* (2.7 Å)

			Cl 1* (3.0 Å)		
-	-	CD5	Occupancy 0.30 B-factor 44.4 Å^2 OE2 Glu88 (2.3 Å) WAT 81 (2.0 Å) WAT 181 (2.2 Å) WAT 187* (2.6 Å)	Occupancy 0.20 B-factor 61.0 Å^2 OE2 Glu 88 (2.3 Å) WAT 313 (2.5 Å) WAT187* (2.7 Å)	-
-	-	CD6	Occupancy 0.40 B-factor 45.3 Å^2 OG Ser131 (2.7 Å) OD1 Asp127 (3.0 Å) WAT 196 (2.5 Å) WAT 197 (2.5 Å) WAT 230 (2.0 Å)	Occupancy 0.40 B-factor 69.3 Å^2 OD1 Asp127 (2.9 Å) WAT 245 (2.5 Å) WAT 311 (2.2 Å)	Occupancy 0.40 B-factor 62.5 Å^2 OD1 Asp127 (2.4 Å) WAT 196 (2.8 Å)
CD4	Occupancy 0.50 B-factor 43.6 Å^2 NE2 His132 (2.2 Å) WAT335 (2.1 Å)	CD7	Occupancy 0.50 B-factor 42.1 Å^2 NE2 His132 (2.5 Å) OD2 Asp135* (2.9 Å) WAT 196 (2.4 Å) WAT 197 (2.5 Å) WAT 275 (1.7 Å)	Occupancy 0.40 B-factor 39.9 Å^2 NE2 His132 (2.7 Å) WAT 245 (2.2 Å) WAT 246 (2.2 Å) WAT 294 (2.1 Å) WAT 295 (2.4 Å)	Occupancy 0.50 B-factor 60.2 Å^2 NE2 His132 (2.7 Å) WAT196 (2.3 Å) WAT197 (2.5 Å) WAT275 (2.4 Å)
CD5	Occupancy 0.30 B-factor 28.2 Å^2 OE1 Glu130 (2.5 Å) OE2 Glu130 (2.5 Å) OE1 Glu130* (2.5 Å) OE2 Glu130* (2.5 Å) OE1 Glu130* (2.5 Å) OE2 Glu130* (2.5 Å)	CD8 at the ternary axis	Occupancy 0.20 B-factor 42.7 Å^2 OE1 Glu130 (2.4 Å) OE1 Glu130* (2.4 Å) OE1 Glu130* (2.4 Å) Cl 2 (1.9 Å) Cl 2* (1.9 Å) Cl 2* (1.9 Å)	Occupancy 0.20 B-factor 46.5 Å^2 OE1 Glu130 (2.5 Å) OE1 Glu130* (2.5 Å) OE1 Glu130* (2.4 Å) Cl 2 (2.3 Å) Cl 2* (2.3 Å) Cl 2* (2.3 Å)	Occupancy 0.30 B-factor 61.3 Å^2 OE1 Glu130 (2.3 Å) OE1 Glu130* (2.3 Å) OE1 Glu130* (2.3 Å) Cl 5 (2.9 Å) Cl 5* (2.9 Å) Cl 5* (2.9 Å)
-	-	CD9	Occupancy 0.40 B-factor 56.5 Å^2 NE2 His114 (2.7 Å) WAT 265* (2.9 Å)	Occupancy 0.20 B-factor 59.1 Å^2 WAT 252* (2.5 Å) Cl 1* (2.9 Å)	Occupancy 0.40 B-factor 72.6 Å^2 NE2 His114 (2.8 Å) WAT 265* (2.8 Å) Cl 5* (2.7 Å)
-	-	CD10	Occupancy 0.30 B-factor 42.1 Å^2 OE1 Glu63/A (2.7 Å) OE2 Glu63/A (2.3 Å) OE2 Glu63/B (2.3 Å) WAT 85 (1.7 Å) WAT 247 (2.5 Å)	Occupancy 0.20 B-factor 51.5 Å^2 OE1 Glu63 (2.6 Å)	Occupancy 0.30 B-factor 62.5 Å^2 OE1 Glu63 (2.9 Å) WAT 85 (2.4 Å) WAT 219 (2.8 Å)
-	-	CD11	Occupancy 0.30 B-factor 30.9 Å^2	Occupancy 0.30 B-factor 33.6 Å^2	Occupancy 0.30 B-factor 25.2 Å^2

			SG Cys48 (2.0 Å) WAT 231 (2.0 Å)	SG Cys48 (2.1 Å) WAT 310 (2.0 Å)	SG Cys48 (2.0 Å) WAT 231 (1.8 Å)
-	-	CD12	Occupancy 0.40 B-factor 56.8 Å^2 OE2 Glu45/B (2.4 Å) WAT 255 (2.2 Å) Cl 5 (2.7 Å)	Occupancy 0.30 B-factor 73.9 Å^2 OE1 Glu45 (2.5 Å) WAT 235 (2.2 Å)	Occupancy 0.40 B-factor 66.7 Å^2 OE2 Glu45 (2.6 Å) WAT 282 (2.9 Å)
CD6	Occupancy 0.35 B-factor 65.1 Å^2 OE1 Glu45/A (2.9 Å) WAT 364 (2.9 Å) WAT 387 (2.0 Å)	CD13	Occupancy 0.20 B-factor 44.1 Å^2 OE1 Glu45/A (2.2 Å) NE2 His49 (2.3 Å)	Occupancy 0.20 B-factor 44.1 Å^2 OE2 Glu45/A (2.5 Å) NE2 His49 (2.7 Å) WAT 236 (2.9 Å)	Occupancy 0.20 B-factor 57.4 Å^2 OE1 Glu45/A (2.2 Å) NE2 His49 (2.5 Å)
CD7	Occupancy 0.20 B-factor 37.4 Å^2 WAT 332 (2.3 Å) WAT 333 (2.4 Å) WAT 332 *(2.3 Å) WAT 333 *(2.4 Å) WAT 332 *(2.3 Å) WAT 333 *(2.4 Å)	-	-	-	-
CD9	Occupancy 0.15 B-factor 42.1 Å^2 OE1 Glu53 (1.9 Å)	-	-	-	-

* Symmetry related residue

Table S4. Anomalous map peak intensities in the structure reported in this work compared to those obtained using crystals of AFt, CDDP-encaspulated AFt and an additional internal control collected using X-ray from a CuKa generator.

Atom name in the Auoxo3-encapsulated AFt	Auoxo3-encapsulated AFt	Corresponding atoms in the structures of CDDP-encapsulated AFt and in the control	CDDP-encapsulated Aft Crystal 1	CDDP-encapsulated Aft Crystal 2	Control	Notes
	Resolution 1.85 Å		Resolution 2.06 Å	Resolution 1.45 Å	Resolution 1.82 Å	
	λ used for data collection 0.15418 nm		λ used for data collection 0.15418 nm	λ used for data collection 0.1065 nm	λ used for data collection 0.1065 nm	Notes
Atom	e/Å^3	***Atom***	e/Å^3	e/Å^3	e/Å^3	
CD1	0.22	***CD1***	0.24	0.28	0.14	
CD2	0.21	***CD2***	0.16	0.12	0.10	
CD8	0.20	***CD3***	0.31	0.10/0.08	0.12	
CD3	1.19	***CD4***	0.92	1.16	0.53	
-	-	***CD5***	-	0.09	0.09	
-	-	***CD6***	0.35	0.12	0.09	
CD4	0.25	***CD7***	0.28	0.17	0.09	
CD5	0.58	***CD8***	0.41	0.15	0.11	
-	-	***CD9***	0.25	0.15	0.10	
-	-	***CD10***	0.30	0.07	0.09	
-	-	***CD11***	0.25	0.06	0.10	
-	-	***CD12***	0.30	0.09	0.10	
CD6	0.22	***CD13***	0.21	0.09	0.16	
CD7	0.36	**-**	-	**-**	-	Not bound to protein residues, but to six water molecule (octahedral

						geometry)
CD9	0.19	**-**	-	**-**	-	Close to Glu53, as in other structures of AFt
Au1	0.76	**-**	-	**-**	-	Close to Cys126
Au2	0.37	**-**	-	**-**	-	Close to Cys48
Au3	0.52	**-**	-	**-**	-	Close to His49
Au4	1.00	**-**	-	**-**	-	Close to Cys126
Au5	3.14	**-**	-	**-**	-	Close to His147
Au6	0.50	**-**	-	**-**	-	Close to Cys48
Au7	0.16	***CPT***	0.21	0.24	-	Close to His132
-	-				-	

Table S5. Distances between main anomalous peaks in the structure of Auoxo3-encapsulated AFt

distance	*Assignment*
3.1 Å	Au2-Au6
3.7 Å	Au1-Au4
3.9 Å	Au3-Au6
5.0 Å	Cd5-Cd7
5.3 Å	Cd2-Cd8
5.3 Å	Au2-Au3
6.2 Å	Au7-Cd4
6.5 Å	Au3-Cd2
6.5 Å	Au3-Cd9
6.6 Å	Cd2-Cd9
7.6 Å	Au1-Cd5
7.7 Å	Au4-Cd5
8.4 Å	Au5-Cd9
9.1 Å	Au6-Cd9
9.5 Å	Au6-Cd6
9.8 Å	Cd4-Cd7

Table S6. Uninterpreted Fo-Fc electron density map peaks in the structure of Auoxo3-encapsulated AFt at level > 5σ

Peak number	e/Å^3	Rmsd (σ)	Note
1	1.08	9.15	Too close to Cd8 (1.9 Å)
2	0.96	8.06	Too close to CD atom of Arg153 (2.2 Å)
3	0.95	7.99	Too close to CE and NE atoms of His114 (0.7 and 0.8 Å, respectively)
4	0.90	7.63	Too close to CD2 atom of His114 (1.9 Å)
5	0.76	6.43	Too close to OD2 atom of Asp127 and to Wat311 (1.8 and 1.4 Å, respectively)
6	0.73	6.17	Too close to OE2 atom of Glu56 and to Cd8 (1.8 and 1.4 Å, respectively)
7	0.71	6.02	On symmetry axis
8	0.67	5.63	Too close to Wat248 (1.5 Å)
9	0.66	5.54	Too close to Wat334 and to OE2 atom of Glu130 (1.9 and 2.3 Å, respectively)
11	0.64	5.37	Too close to Wat382 (1.7 Å)
12	0.63	5.32	Too close to Wat386 (1.3 Å)
13	0.63	5.29	Too close to CE atom of Met96 (< 0.3 Å)
14	0.63	5.28	Too close to Au4 and to Wat 373 (1.5 and 1.8 Å, respectively)
15	0.61	5.14	Too close to CD and OE atoms of Glu63 (1.8 and 1.7 Å, respectively)
16	0.61	5.13	Too close to Wat 334 (1.7 Å)
17	0.60	5.05	Too close to OE1 atom of Glu57 and to Wat358 (2.1 and 1.3 Å, respectively)

Table S7. Cellular uptake of Au associated with Auoxo3-encaspulated AFt by MCF-7 cells during 24, 48 and 72 h normalized to 1x 10^6 cells.*

	24h	48h	72h
Sample			
	Au (%)	Au (%)	Au (%)
Total amount	100	100	100
Cell conditioned medium	87.5	71.4	68.4
Cell washing	3.1	1.2	3.6
Cell lysate	9.0	11.9	21.6

*Average of two different measurements. Errors about 10%.

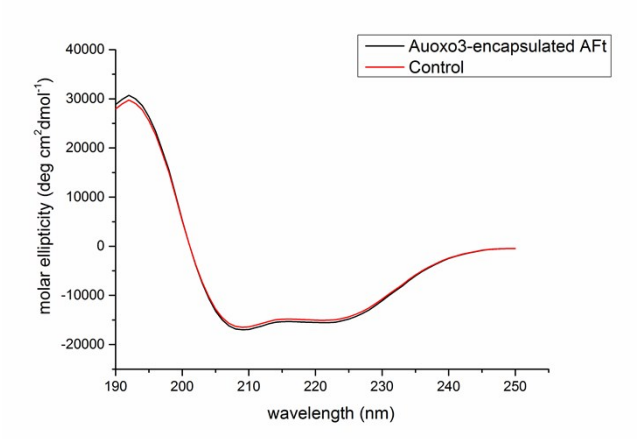

Figure S1. Far-UV CD spectra of Auoxo3-encapsulated AFt (black) compared to the control (red).

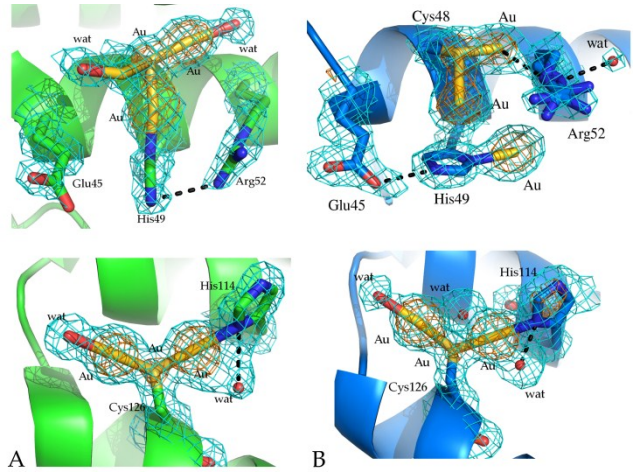

Figure S2. Comparison between Au binding sites observed in the structure of horse liver ferritin with $AuCl_4^-$ (A) and in Auoxo3-encapsulated AFt (B). 2Fo-Fc electron density maps are contoured at 1σ (cyan) and 4 σ (orange). The structure of horse liver ferritin with $AuCl_4^-$ is coloured in green; the structure of Auoxo3-encapulstaed Aft is coloured in cyan

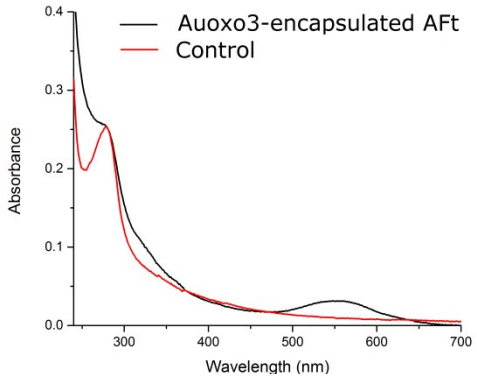

Figure S3. UV-vis absorption spectra of 0.25 mg x mL^{-1}Auoxo3-encapsulated AFt (black) compared to the control (red). The absorption differences between 250 and 280 nm and the appearance of a peak at 548 nm in aged samples confirm that Auoxo3 was successfully encapsulated in the AFt nanocage and suggest that a small amount gold nanoparticles could be formed in Auoxo3-encapsulated AFt sample.

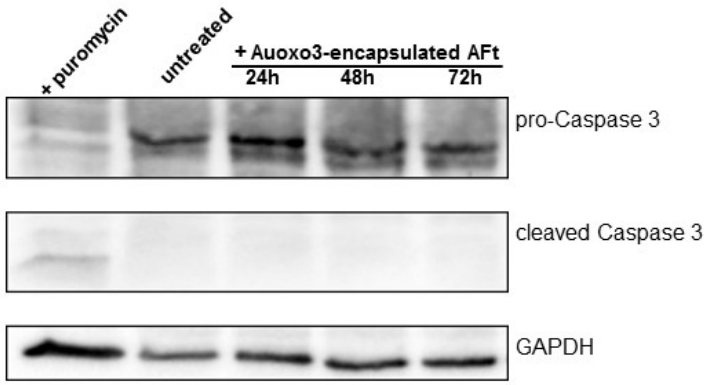

Figure S4. Detection of apoptosis in Auoxo3-encapsulated AFt-treated MCF-7 cells. MCF-7 cells were pre-incubated with 0.4 μg/mL Auoxo3-encapsulated AFt for 24, 48 and 72 h. Western blot was performed using anti-Caspase 3, which recognizes both pro-Caspase 3 and the activated form. GAPDH was used as loading control. A positive control was obtained by incubating cells in the presence of 50 μg/mL puromycin for 24 h.

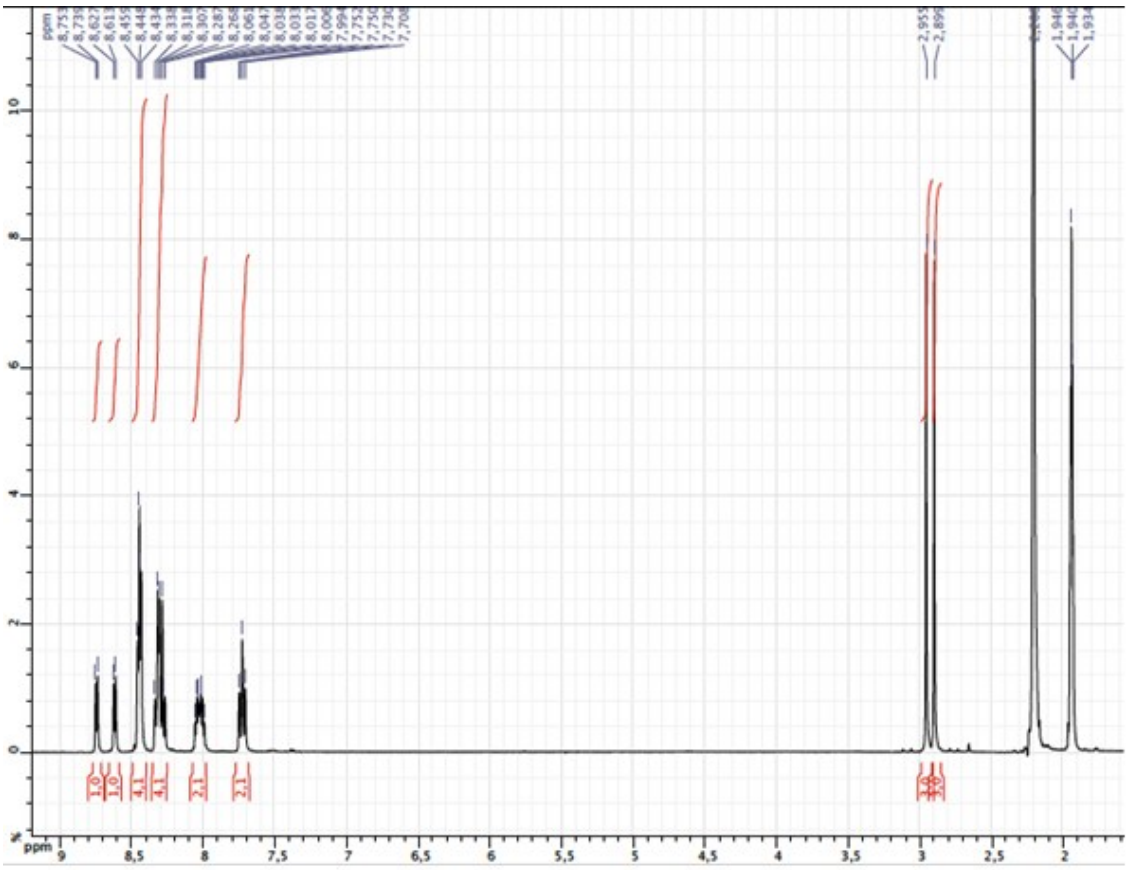

Figure S5. ^{1}H NMR (CD_3CN, 400 MHz) of Auoxo3 recovered from reaction with NaOH 0.1M